

Acknowledgements

This work was completed while A.G. was a graduate student in the MIT/WHOI Joint Program in Physical Oceanography. We thank J. Toole, B. Warren, J. Marotzke, D. Glover and N. Hogg, B. Arbic, G. McKinley, A. Czaja, A. Macdonald, J. Marshall and M. Fieux also provided helpful comments on the manuscript. We are grateful to the principal investigators who provided the data from the World Ocean Circulation Experiment and the Franco-Indonesian Java-Australia Dynamic Experiment. G. Brown and D. Spiegel helped to design the figures. We were supported by the Jet Propulsion Laboratory and by gifts from Ford, General Motors and Daimler-Chrysler to MIT's Climate Modelling Initiative. This work is a contribution to the World Ocean Circulation Experiment.

Correspondence and requests for materials should be addressed to A.G. (e-mail: ganacho@ifremer.fr).

The use of earthquake rate changes as a stress meter at Kilauea volcano

James Dieterich^{*}, Valérie Cayol^{†*} & Paul Okubo[‡]

^{*} US Geological Survey, Menlo Park, California 94025, USA

[†] Université B. Pascal, Clermont Ferrand, France

[‡] Hawaiian Volcano Observatory, US Geological Survey, Hawaii 96718, USA

Stress changes in the Earth's crust are generally estimated from model calculations that use near-surface deformation as an observational constraint. But the widespread correlation of changes of earthquake activity with stress¹⁻⁵ has led to suggestions that stress changes might be calculated from earthquake occurrence rates obtained from seismicity catalogues. Although this possibility has considerable appeal, because seismicity data are routinely collected and have good spatial and temporal resolution, the method has not yet proven successful, owing to the non-linearity of earthquake rate changes with respect to both stress and time. Here, however, we present two methods for inverting earthquake rate data to infer stress changes, using a formulation for the stress- and time-dependence of earthquake rates⁶. Application of these methods at Kilauea volcano, in Hawaii, yields good agreement with independent estimates, indicating that earthquake rates can provide a practical remote-sensing stress meter.

The inversions use a formulation for earthquake rate changes⁶ derived from laboratory observations of rate- and state-dependent fault strength⁶⁻⁸, which constrain the earthquake nucleation process to be dependent on both time and stress. Previously, this formulation has been applied to model the spatial and temporal characteristics of earthquake clustering phenomena, including foreshocks and aftershocks^{6,7}, and to evaluate earthquake probabilities following large earthquakes⁹. The effectiveness of the formulation for forward modelling of earthquake phenomena, and its derivation from observed fault properties, provide the basis for its use to estimate stress changes from earthquake rate data. This approach yields stresses that drive the earthquake process. As such, it is distinct from other seismological methods that yield measures of stress changes resulting from earthquakes.

The formulation of Dieterich⁶ for rate of earthquake activity R (in a specified magnitude range) can be written in the condensed form

$$R = \frac{r}{\gamma \dot{S}_r}, \text{ where } d\gamma = \frac{1}{A\sigma} [dt - \gamma dS] \quad (1)$$

where γ is a state variable, t is time, and S is a modified Coulomb stress function defined below. The constant r is the steady-state earthquake rate at the reference stressing rate \dot{S}_r . A is a dimensionless fault constitutive parameter with values usually in the range 0.005–0.015 (refs 6–8). The modified Coulomb stress function is defined as

$$S = \tau - [\mu - \alpha]\sigma \quad (2)$$

where τ is the shear stress acting across fault planes that generate earthquakes (positive in the slip direction), σ is the normal stress (less pore fluid pressure), μ is the coefficient of fault friction and α is a constitutive parameter^{6,10} with an assigned value in this study of 0.25 (refs 6, 10). In equation (1), the term $A\sigma$ is a constant (that is, changes in σ are negligible relative to total σ). For a stress step, equation (1) yields the characteristic aftershock sequence, which consists of an immediate jump of seismicity rate followed by decay that obeys the Omori t^{-1} aftershock decay law with aftershock duration $t_a = A\sigma/\dot{S}$ (ref. 6).

We use two methods to estimate stress changes from earthquake rate data. The first gives stress as a function of time in a specified volume. From equation (1), the observed rate R is used to directly calculate γ as a function of time (that is, $\gamma(t) = r/R(t)\dot{S}_r$). This requires an estimate of \dot{S}_r , which can be obtained from independent

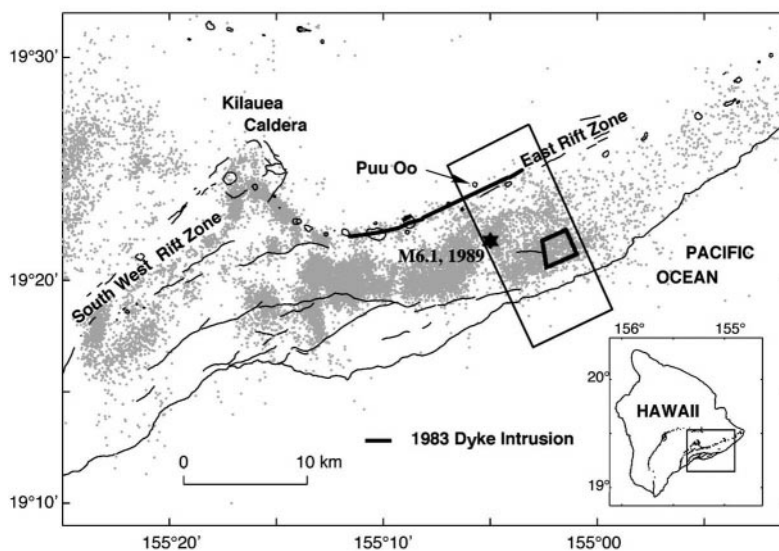


Figure 1 Map of Kilauea volcano showing earthquakes of magnitude $M \approx 1.5$ from 1976 to 1983. Intrusion of magma into the southwest and east rift zones of Kilauea causes rift expansion, and results in motion of the south flank to the SSE. Eruptive fissures initiated

the Puu Oo eruption, which started 1 January 1983 and continues to the present. The small polygon is the region of analysis of Fig. 2; the large rectangle gives the region of analysis of Figs 3 and 4.

observations of deformation rates, or from observations of after-shock decay using the relation given above for aftershock duration. Stress changes over successive time intervals are then obtained using the solution of equation (1) for a stress step at the mid-point of a time interval

$$\Delta S = A\sigma \ln \left[\frac{\gamma_i + \frac{\Delta t}{2A\sigma}}{\gamma_{i+1} - \frac{\Delta t}{2A\sigma}} \right] \quad (3)$$

where γ_i and γ_{i+1} are the estimated values of γ at the beginning and end, respectively, of the time step Δt .

The second method gives the spatial distribution of stress changes for a stress event, such as an earthquake mainshock or a magmatic intrusion. This method uses the solution of equation (1) for a history that consists of constant stressing at \dot{S}_r , followed by a stress step ΔS (the stress event), followed by constant stressing at \dot{S}_r . Solving equation (1) for this stressing history, and integrating the rates to obtain the expected number of events in time intervals, gives

$$\Delta S = A\sigma \ln \left\{ \frac{\dot{S}_r [\exp(N_2 \dot{S}_r t_2 / N_1 A\sigma) - 1]}{\dot{S}_r [\exp(\dot{S}_r t_1 / A\sigma) - 1]} \right\} \quad (4)$$

where N_1 is the count of earthquakes in time interval t_1 immediately before the stress event, and N_2 is the earthquake count in interval t_2 immediately following the event. As is usual in Coulomb stress

analysis, ΔS depends on fault orientation and slip direction. Consequently, in solving equation (4) for stress, counts of earthquakes (sorted by fault orientation) are made for sub-regions centred on grid points.

The south flank of Kilauea volcano, Hawaii, was chosen for this initial application of these methods for two reasons: first, this region experiences frequent stressing events from well studied causes, and second, various deformation observations have been made that can provide independent estimates of stress changes. This region is undergoing rapid deformation due to expansion of the active rift zones, and has high rates of seismic activity (Fig. 1). Since 1983, measured rates of south flank displacement^{11,12}, to the SSE, have ranged between 6 and 20 cm yr⁻¹. Expansion of the rift zones occurs by two mechanisms: (1) continuous slow intrusion of magma into a deep dyke-like body^{13,14}; and (2) rapid intrusion events that emplace shallow dykes, which sometimes form eruptive fissures^{11-13,15,16}. Rift zone expansion is coupled to, and accommodated by, fault slip at the interface between the volcano and the pre-existing sea floor¹⁶⁻¹⁸. The magnitude 6.1 earthquake of 25 June 1989, and numerous moderate and small earthquakes, occurred within the region of this study¹⁸⁻²⁰.

We have examined stresses in several sub-regions of the south flank of Kilauea using the method based on equation (3). The area indicated by the small polygon in Fig. 1 displays examples of seismicity and stress changes—shown in Fig. 2a and b, respec-

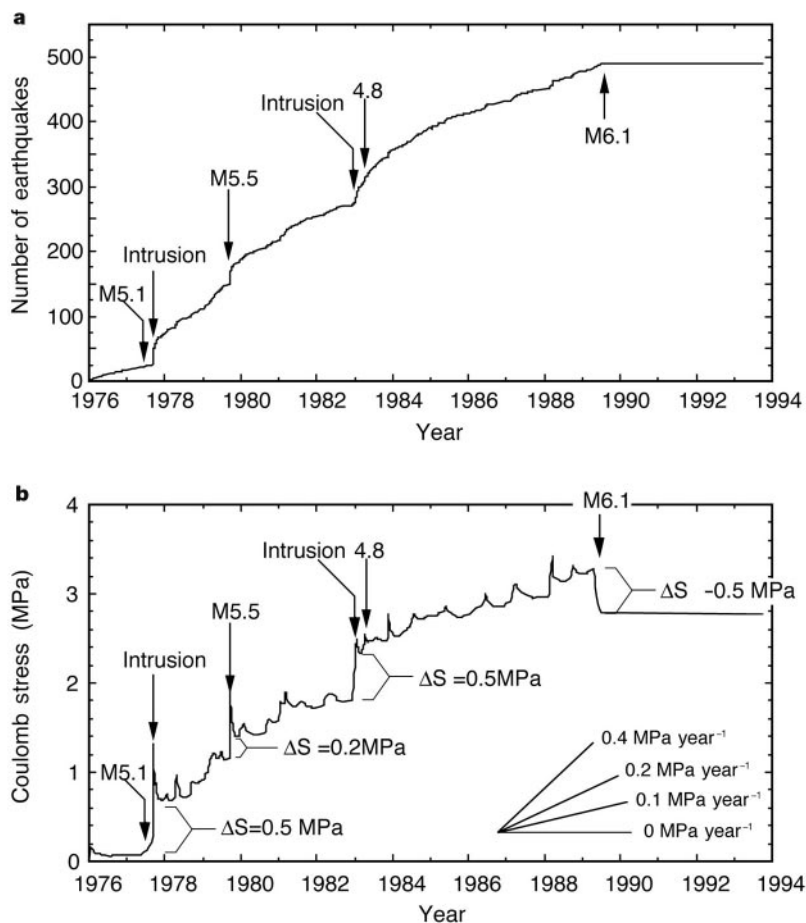


Figure 2 Earthquakes and stresses for the small polygon shown in Fig. 1. **a**, Cumulative number of earthquakes of magnitude $M \approx 1.5$ in the depth range 5–13 km. Transient changes of earthquake rates followed intrusion events of 1977 and 1983, the 1979 magnitude 5.5 earthquake, and the 1989 magnitude 6.1 earthquake. **b**, Stresses obtained from earthquake rates. A low pass filter was used to smooth short-term fluctuations in rate before calculating the stresses using equation (3) in the text. We

assume $A = 0.005$, σ equal to the overburden pressure less hydrostatic pore-fluid pressure using a bulk density of $\rho = 2.3$ for the rubby lava flows of the volcano flank. These give a nominal value for $A\sigma = 0.45$ MPa at the representative earthquake depth of 7 km. The inversion employs $\dot{S}_r = 0.3$ MPa yr⁻¹; this value was obtained from the observed decay of earthquakes following the 1977 intrusion using the relation $t_a = A\sigma/\dot{S}_r$.

tively—that are representative of the region. At the times of the rift intrusion/eruption events of 12 September 1977 and 1 January 1983, and the magnitude 5.5 earthquake of 21 September 1979, seismic activity sharply increased and then decayed to a background rate following the t^{-1} Omori decay law. These seismicity changes

give Coulomb stress increases of about 0.5 MPa for the 1977 and 1983 intrusions. As discussed below, these stress changes are consistent with estimates from boundary element models constrained by geodetic data. The seismicity jump at the time of the 1979 earthquake gives a stress increase of 0.2–0.5 MPa. This is consistent with stresses obtained from elastic dislocation calculations for an earthquake of that magnitude at that distance (3–4.5 km distance, 2 km rupture radius, and 3 MPa stress drop). Aftershocks to the magnitude 6.1 earthquake of 25 June 1989 occurred on three sides of the polygon shown in Fig. 1, and gave stress increases of 0.3–0.6 MPa, but within the area shown, earthquake activity ceased following the 1989 mainshock. It is our interpretation that the polygon lies within a region of stress drop for the 1989 earthquake. The stress drop of 0.5 MPa in Fig. 2b is the minimum needed to reduce the rate to less than one event in the 5 years following the mainshock.

Various factors, including random fluctuations in earthquake rates and possible catalogue inconsistencies during swarm activity, can introduce artefacts into the inversions that can be confused with short-term stress changes. Consequently, short-term stress fluctuations shown in Fig. 2 should be treated with caution. However, long-term stressing rate changes and stress steps appear to be well resolved. The stress solution of Fig. 2b indicates a slowing of stressing rates, from about 0.30 MPa yr⁻¹ to about 0.15 MPa yr⁻¹, sometime between 1981 and 1983. This slowing is consistently seen for other polygons SSE of the 1983 event, and corresponds to a previously recognized¹¹ decrease of surface deformation rates over much of the south flank around the time of the 1983 intrusion, apparently because the continuing volcanic eruption decreased the supply of magma intruded into the rift.

Independent estimates of stress changes before the 1983 intrusion, and of stress changes resulting from it, are obtained from three-dimensional boundary element models^{20,21}; these stress changes are shown in Figs 3a and b, respectively. The models satisfy extensive deformation data sets before, and spanning, the 1983 intrusion; these data include horizontal displacements from trilateration measurements, level line data across the rift zone, and tide gauge data. In addition, the models incorporate topographic effects and the coupled interactions between the rift zone and the decollement fault at the base of the volcano. Before the 1983 intrusion event, earthquakes within the south flank concentrated in regions

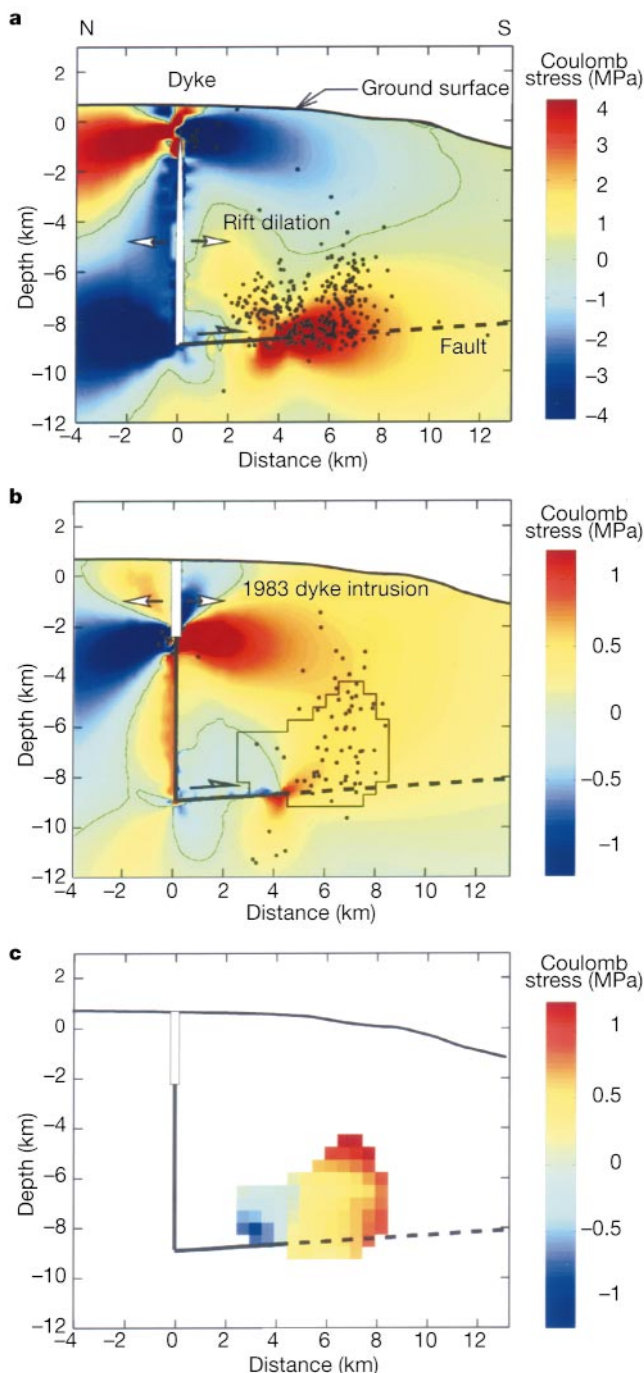


Figure 3 Earthquakes of magnitude $M \approx 1.5$ and Coulomb stress scale on a cross-section along the midline of the large box shown in Fig. 1. Coulomb stresses are calculated for faults that are parallel to the basal fault with slip perpendicular to the rift. Positive stress favours slip allowing rift expansion (arrows), and negative stress inhibits slip. The creeping section of the basal fault is shown as a solid line and the locked portion by a dashed line. **a**, Earthquakes and Coulomb stresses for the three years before the 1 January 1983 intrusion event and eruption²¹. **b**, Earthquakes for the 90 d following the 1 January 1983 eruption. Coulomb stress changes for the intrusion event are calculated for a pressurized dyke that extends to the surface to give the observed 2-m extension of trilateration lines that cross the rift zone. **c**, Stress changes obtained from the earthquake data using equation (4) in the text.

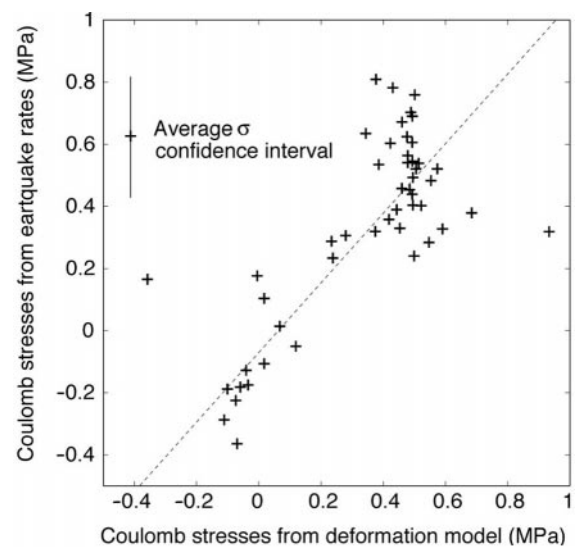


Figure 4 Comparison of stresses calculated from the boundary element model of the 1983 intrusion event (Fig. 3b) with the stresses calculated from the seismicity rate changes (Fig. 3c). Only the better-quality earthquake-derived stresses with $(N_1 + N_2) \approx 45$ (see text) are shown.

where stresses, resulting from slow inflation of the deep rift zone, are high (Fig. 3a). At the time of the shallow intrusion, the rift opened about 2 m (refs 11, 15, 21), an eruptive fissure formed (Fig. 1), and seismicity within this region of the south flank immediately increased by more than a factor of ten (Fig. 2a). The intrusion also resulted in changes in the patterns of stressing and seismic activity (Fig. 3a, b). Relative to the pre-intrusion period, seismic activity shifted away from the rift and more shallow events occurred. These changes are consistent with stresses that we have calculated for the 1983 intrusion (Fig. 3b). That is, the regions of increased and decreased earthquake rates correspond to regions of increased and decreased stress, respectively, resulting from the intrusion.

We believe that the boundary element model of the 1983 intrusion is also a reasonable representation of the stress changes for the 1977 intrusion. Each occurred in the same region^{15,20}, each resulted in very similar changes in seismicity patterns and rates, and the limited deformation data for the 1977 event are consistent with the more extensive 1983 data set.

Figure 3c gives the distribution of stress changes for the 1983 intrusion obtained from the seismicity data using equation (4). Counts of earthquakes for this calculation are made on a square grid with 0.5-km spacing of centres, over a radius of 1 km. A three-year period, t_1 , was used for counts before the event (N_1), and 90 days, t_2 , was used for counts following the event (N_2). We use the stressing rate results for the small polygon in Fig. 1 to set $\dot{\sigma}_r = 0.3 \text{ MPa yr}^{-1}$ before intrusion and $\dot{\sigma}_r = 0.15 \text{ MPa yr}^{-1}$ following the intrusion. Additionally, the parameter $A\sigma$ is made depth-dependent by allowing σ to increase with depth by the weight of the overburden less hydrostatic pore-fluid pressure.

For the region of the small polygon (Fig. 1), the boundary element model gives a stress increase of 0.3–0.6 MPa for the 1983 intrusion. This compares well with the seismicity-based stress change of 0.5 MPa obtained for both the 1977 and 1983 intrusion events using equation (3) (Fig. 2b). The pattern and magnitudes of stress changes at the time of the 1983 intrusion obtained from earthquake data using equation (4) (Fig. 3c) are in agreement with the boundary element calculation (Fig. 3b). Regression of the Coulomb stresses from the boundary element model of the intrusion against stresses from equation (4) has a slope of 1.1, and the correlation coefficient is 0.80 (Fig. 4).

In summary, seismicity changes coincide with documented deformation events for the south flank of Kilauea volcano. Inversions of earthquake rates for stress changes based on equation (1) give consistent results that agree with other estimates of stress. An additional internal consistency check of the earthquake rate formulation is provided by the previously described slowing of deformation rates that began around 1981–1983. As noted above, equation (1) predicts an inverse relationship between stressing rate and the time t_a for seismicity to decay to the background rate following a stress step. As the data of Fig. 2a show, the time for seismicity to return to a background rate following the 1983 intrusion is about twice as long as that following the 1977 intrusion; this is consistent with a halving of the stressing rate.

The methods presented here provide a way to use seismicity rate information in earthquake catalogues as a stress meter. This approach is able to resolve both positive and negative stress steps, as well as long-term changes in stressing rate. Because this approach does not depend on previous models of specific structures, it can also provide constraints on the models used to analyse observations of deformation. □

Received 22 March; accepted 24 August 2000.

1. Simpson, R. W. & Reasenber, P. A. Earthquake induced stress changes on central California faults. *US Geol. Surv. Prof. Pap.* **1550-F**, 55–89 (1994).
2. King, G. C. P., Stein, R. S. & Lin, J. Static stress changes and the triggering of earthquakes. *Bull. Seismol. Soc. Am.* **84**, 935–953 (1994).
3. Jaumé, S. C. & Sykes, L. R. Evolution of moderate seismicity in the San Francisco Bay region, 1850 to 1993; Seismicity changes related to the occurrence of large and great earthquakes. *J. Geophys. Res.* **101**, 765–789 (1996).

4. Harris, R. A., Simpson, R. W. & Reasenber, P. A. Influence of static stress changes on earthquake locations in southern California. *Nature* **375**, 221–224 (1995).
5. Stein, R. S. The role of stress transfer in earthquake occurrence. *Nature* **402**, 605–609 (1999).
6. Dieterich, J. H. A constitutive law for rate of earthquake production and its applications to earthquake clustering. *J. Geophys. Res.* **99**, 2601–2618 (1994).
7. Dieterich, J. H. & Kilgore, B. Implications of fault constitutive properties for earthquake prediction. *Proc. Natl Acad. Sci. USA* **93**, 3787–3794 (1996).
8. Scholz, C. H. Earthquakes and friction laws. *Nature* **391**, 37–42 (1998).
9. Stein, R. S., Barka, A. A. & Dieterich, J. H. Progressive failure on the North Anatolian fault since 1939 by earthquake stress triggering. *Geophys. J. Int.* **128**, 594–604 (1997).
10. Linker, M. F. & Dieterich, J. H. Effects of variable normal stress on rock friction: observations and constitutive equations. *J. Geophys. Res.* **97**, 4923–4940 (1992).
11. Delaney, P. T., Miklius, A., Arnadottir, T., Okamura, A. & Sako, M. Motions of Kilauea volcano during sustained eruption from the Puu Oo and Kapaianaha vents, 1983–1991. *J. Geophys. Res.* **98**, 17801–17820 (1993).
12. Owen, S. P. *et al.* Rapid deformation of the south flank of Kilauea volcano, Hawaii. *Science* **267**, 1328–1332 (1995).
13. Delaney, P. T., Fiske, R. S., Miklius, Okamura, A. & Sako, M. Deep magma body beneath the summit and rift zones of Kilauea volcano. *Science* **247**, 1311–1316 (1990).
14. Gillard, D., Rubin, A. M. & Okubo, P. Highly concentrated seismicity caused by deformation of Kilauea's deep magma system. *Nature* **384**, 343–346 (1996).
15. Dvorak, J. J. *et al.* Mechanical response of the south flank of Kilauea volcano, Hawaii, to intrusive events along the rift zones. *Tectonophysics* **124**, 193–209 (1986).
16. Dieterich, J. H. Growth and persistence of Hawaiian volcanic rift zones. *J. Geophys. Res.* **93**, 4258–4270 (1988).
17. Ando, M. The Hawaiian earthquake of November 29, 1975: Low dip angle faulting due to forceful injection of magma. *J. Geophys. Res.* **84**, 7616–7626 (1979).
18. Got, J., Fréchet, J. & Klein, F. W. Deep fault plane geometry inferred from multiplet relative relocation beneath the south flank of Kilauea. *J. Geophys. Res.* **99**, 15375–15386 (1994).
19. Klein, F. W., Koyanagi, R. Y., Nakata, J. S. & Tanigawa, W. R. The seismicity of Kilauea's magma system. *US Geol. Surv. Prof. Pap.* **1350**, 1019–1185 (1987).
20. Cayol, V. & Cornet, F. H. 3D mixed boundary elements for elastostatic deformation field analysis. *Int. J. Rock Mech. Min. Sci.* **34**, 275–287 (1997).
21. Cayol, V., Dieterich, J. H., Okamura, A. T. & Miklius, A. High rates of deformation prior to the 1983 Eruption of Kilauea Volcano, Hawaii. *Science* **288**, 2343–2346 (2000).

Acknowledgements

We thank A. Rubin for useful suggestions for this manuscript.

Correspondence and requests for materials should be addressed to J.D. (e-mail: jd Dieterich@usgs.gov).

Concurrent density dependence and independence in populations of arctic ground squirrels

Tim J. Karels & Rudy Boonstra

Division of Life Sciences, University of Toronto at Scarborough, 1265 Military Trail, Scarborough, Ontario, M1C 1A4, Canada

No population increases without limit. The processes that prevent this can operate in either a density-dependent way (acting with increasing severity to increase mortality rates or decrease reproductive rates as density increases), a density-independent way, or in both ways simultaneously^{1–3}. However, ecologists disagree for two main reasons about the relative roles and influences that density-dependent and density-independent processes have in determining population size^{4,5}. First, empirical studies showing both processes operating simultaneously are rare⁶. Second, time-series analyses of long-term census data sometimes overestimate dependence^{7,8}. By using a density-perturbation experiment^{9–12} on arctic ground squirrels, we show concurrent density-dependent and density-independent declines in weaning rates, followed by density-dependent declines in overwinter survival during hibernation. These two processes result in strong, density-dependent convergence of experimentally increased populations to those of control populations that had been at low, stable levels.